Hindawi Publishing Corporation
Journal of Nanomaterials
Volume 2014, Article ID 694073, 8 pages
http://dx.doi.org/10.1155/2014/694073

Research Article

Multiwalled Carbon Nanotube-TiO_2 Nanocomposite for Visible-Light-Induced Photocatalytic Hydrogen Evolution

Ke Dai,[1] Xiaohu Zhang,[2] Ke Fan,[2] Peng Zeng,[2] and Tianyou Peng[2]

[1] *College of Resources and Environment, Huazhong Agricultural University, Wuhan 430070, China*
[2] *College of Chemistry and Molecular Science, Wuhan University, Wuhan 430072, China*

Correspondence should be addressed to Ke Dai; dk@mail.hzau.edu.cn and Tianyou Peng; typeng@whu.edu.cn

Received 15 May 2014; Revised 5 July 2014; Accepted 17 July 2014; Published 10 August 2014

Academic Editor: Xiaohu Huang

Multiwalled carbon nanotube- (MWCNT-) TiO_2 nanocomposite was synthesized via hydrothermal process and characterized by X-ray diffraction, UV-vis diffuse reflectance spectroscopy, field emission scanning electron microscope, thermogravimetry analysis, and N_2 adsorption-desorption isotherms. Appropriate pretreatment on MWCNTs could generate oxygen-containing groups, which is beneficial for forming intimate contact between MWCNTs and TiO_2 and leads to a higher thermal stability of MWCNT-TiO_2 nanocomposite. Modification with MWCNTs can extend the visible-light absorption of TiO_2. 5 wt% MWCNT-TiO_2 derived from hydrothermal treatment at 140°C exhibiting the highest hydrogen generation rate of 15.1 μmol·h^{-1} under visible-light irradiation and a wide photoresponse range from 350 to 475 nm with moderate quantum efficiency (4.4% at 420 nm and 3.7% at 475 nm). The above experimental results indicate that the MWCNT-TiO_2 nanocomposite is a promising photocatalyst with good stability and visible-light-induced photoactivity.

1. Introduction

Hydrogen resource obtained directly from water splitting using photocatalyst and solar light is under scrutiny as a clean energy resource; however it has been facing technical challenge to find a stable and efficient photocatalyst that can maximally utilize solar light [1]. In addition to oxide semiconductors, a great variety of novel photoactive semiconductors have been developed in the last few years. Among these, mixed oxides of transition metal like Nb, V, or Ta or with main group elements such as Ga, In, Sb, or Bi have been extensively investigated as attractive candidates for visible-light-induced photocatalysis [2]. Also, sulfides and nitrides of different metals have been frequently selected to obtain materials with visible-light-driven photoactivity [3]. Titania (TiO_2) is a widely used photocatalyst due to its high chemical stability, low cost, and nontoxic nature [4], but it can only absorb UV light with low quantum efficiency due to its wide bandgap (*ca.* 3.2 eV), which limits its application in visible-light-driven photocatalysis. The above problems have been partly resolved by many methods, such as surface modification via organic materials [5], semiconductor coupling [6], bandgap modification by nonmetals [7, 8], and plasmonic metal (Ag and Au) doping [9–14], creating oxygen vacancies and disorder or dye sensitization [15–17].

Due to the special structures and extraordinary mechanical and unique electronic properties, carbon nanotubes (CNTs) have the potential to extend the photoresponse range of TiO_2 to visible-light region by modification of bandgap and/or sensitization and increase the photoactivity of TiO_2 by contribution to high surface area and inhibition of electron-hole recombination [18]. Single-walled carbon nanotubes (SWCNTs) have shown a synergy effect on enhancing photoactivity for H_2 evolution over a mixture of SWCNTs and TiO_2 [19]. Ou et al. [20] have also demonstrated that multiwalled carbon nanotubes (MWCNTs) could enhance the visible-light-driven photoactivity of TiO_2 by acting as a photosensitizer in the MWCNT-TiO_2 : Ni composite. MWCNT-TiO_2 nanocomposite with visible-light-driven photoactivity was successfully synthesized via direct growth of TiO_2 nanoparticles on the surface of the functionalized MWCNTs by the hydrothermal treatment in our group [21]. However, the effects of MWCNT pretreatment, MWCNT content, and

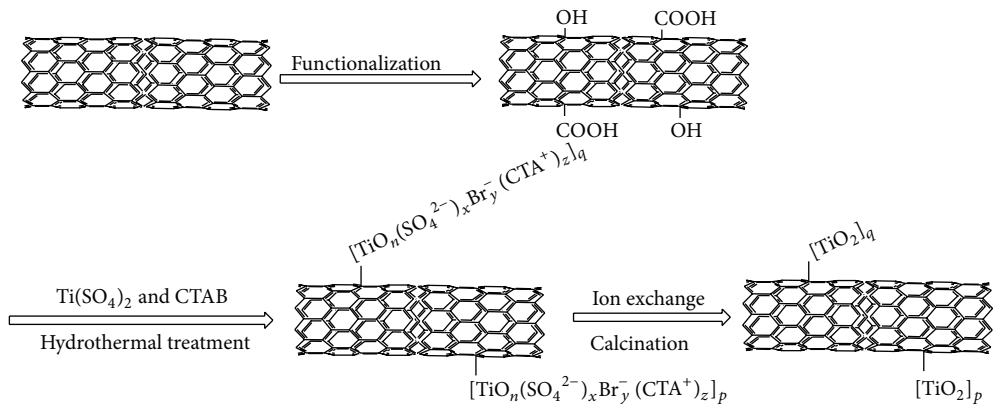

Figure 1: Schematical formation model for MWCNT-TiO_2 nanocomposite.

synthetic conditions of MWCNT-TiO_2 nanocomposite on its photocatalytic hydrogen evolution efficiency and quantum efficiency under monochromatic light irradiation are still beyond our knowledge.

Herein, MWCNT-TiO_2 nanocomposite was synthesized, characterized, and employed for photocatalytic H_2 production from triethanolamine (TEOA) solution. The effects of pretreatment methods, content of MWCNTs, and hydrothermal temperature on the photocatalytic H_2 evolution efficiency over the Pt-loaded photocatalysts were studied. Moreover, the apparent quantum efficiency (AQE) of 5 wt% MWCNT-TiO_2 upon incident monochromatic light is also investigated.

2. Experiment

2.1. Pretreatment Methods for MWCNTs. MWCNTs (diameter < 8 nm; length 10–30 μm; purity > 95 wt%) were purchased from Chengdu Organic Chemicals (Chinese Academy Science, China), and were functionalized by different methods: the as-received MWCNTs were chemically oxidized in a mixture of sulfuric acid and nitric acid (3/1, v/v) while being ultrasonicated for 2 h (Method A [22]); the as-received MWCNTs were treated in boiled nitrate solution (20 wt%) for 1 h for surface functionalization (Method B [21]); the as-received MWCNTs were dispersed in 5.0 M HNO_3 solution and refluxed for 48 h at 140°C (Method C). These functionalized MWCNTs were washed with water to neutral, dried under vacuum, and denoted as MWCNT (A), MWCNT (B), and MWCNT (C), respectively.

2.2. Preparation and Characterization of MWCNT-TiO_2 Nanocomposites. All other chemical reagents used in the study were of analytical grade and used without further purification, unless stated otherwise. The preparation procedure for MWCNT-TiO_2 nanocomposites is demonstrated in Figure 1. In a typical experiment, pretreated MWCNTs were ultrasonically dispersed in deionized water, and then titanium sulfate ($Ti(SO_4)_2$) was added into the dispersion under stirring. The obtained mixture was added into cetyltrimethylammonium bromide (CTAB) solution under the molar ratio of $Ti(SO_4)_2 : CTAB : H_2O$ is 1 : 0.12 : 100. After stirring, the resulting mixture (pH 0.2) was aged at room temperature for 12 h and then transferred into an autoclave for 72 h hydrothermal treatment at 100°C. The resulting materials were collected using the centrifugation technique and mixed with a water and ethanol (molar ratio 1 : 1) solution of sodium chloride under stirring at 40°C for 5 h. Resultant sample was washed with water and ethanol, dried at 80°C overnight, and calcined at 400°C for 5 h.

X-ray diffraction (XRD) patterns were obtained on a XRD-6000 diffractometer using Cu Kα as radiation (λ = 0.15418 nm). Scanning electron microscope (SEM) observation was conducted on a JEOL-6700F electron microscope. Diffuse reflectance spectra (DRS) were recorded on a Cary 5000 UV-Vis-NIR spectrophotometer equipped with an integrating sphere (Varian, USA). Thermogravimetry (TG) curves were recorded on a STA 449C thermal analyzer (Netzsch, Germany). The Brunauer-Emmett-Teller (BET) surface areas were analyzed by nitrogen adsorption-desorption measurement using a Micromeritics ASAP 2020 apparatus after the samples were degassed at 180°C.

2.3. Photocatalytic Activity Measurement. The obtained MWCNT-TiO_2 nanocomposite was loaded with Pt and tested for its photocatalytic activity through a photocatalytic hydrogen evolution system as described in our previous publication [21, 23]. A 300 W Xe-lamp (PLS-SXE300C, Beijing Trusttech Co., Ltd., China) was applied as the light source, which was collimated and focalized into 5 cm^2 parallel faculae. A cut-off filter (Kenko, L-42; λ > 420 nm) was employed to obtain the visible-light irradiation (λ > 420 nm). The reaction was performed in a water suspension which contains 85 mL water, 15 mL triethanolamine (TEOA), and 40 mg photocatalyst. The suspension was irradiated from top of the system after thoroughly removing air. H_2 production rate was analyzed with a gas chromatograph (GC, SP-6800A, TCD detector, 5 Å molecular sieve columns, and Ar carrier).

The apparent quantum efficiency (AQE) was measured under the same photocatalytic reaction condition except for

Table 1: Summary of the physicochemical properties of MWNT and MWNT-TiO_2 nanocomposite.

Sample	Crystal size[a] (nm)	C_{TG}[b] (wt%)	S_{BET} (m^2/g)	Mean pore size[c] (nm)	Total volume[d] (cm^3/g)
1.25 wt% MWNT-TiO_2	12.8	1.5	110.8	10.9	0.35
2.5 wt% MWNT-TiO_2	12.1	3.2	97.5	12.4	0.36
5 wt% MWNT-TiO_2	12.9	5.7	79.8	12.1	0.28
10 wt% MWNT-TiO_2	12.6	9.9	110.1	11.8	0.37
20 wt% MWNT-TiO_2	11.8	18.5	166.7	9.1	0.42
MWNT	—	—	392.5	7.6	0.74

[a]Calculated by the Scherrer equation.
[b]Carbon content determined by TGA-DSC analyses.
[c]Average pore diameter calculated from BJH desorption average pore width (4 V/A).
[d]Single point total pore volume at the relative pressure of *ca.* 0.995.

the incident monochromatic light wavelength. The hydrogen yields of 1 h photocatalytic reaction under visible-light with different wavelengths of 350, 365, 380, 420, 435, 450, 475, 500, 520, and 550 nm were measured. Each run was carried out three times and the average value was taken (the relative errors are under 10%). The band-pass and cut-off filters and a calibrated Si photodiode (SRC-1000-TC-QZ-N, Oriel, USA) were used in measurement. Apparent quantum efficiencies at different wavelengths were calculated by the following equation:

$$\begin{aligned}\text{AQE (\%)} &= \frac{\text{The number of reacted electrons}}{\text{The number of incident photons}} \times 100 \\ &= \frac{2 \times \text{The number of evolved } H_2 \text{ molecules}}{\text{The number of incident photons}} \times 100.\end{aligned} \quad (1)$$

3. Results and Discussion

Figure 2 shows the XRD patterns of MWCNT, TiO_2, and various MWCNT-TiO_2 nanocomposites. As can be seen from Figure 2(a), the main diffraction peaks of various products can be ascribed to anatase TiO_2, whereas a decrease in the crystallinity of anatase can be found after the introduction of MWCNTs, indicating the decrease in the grain size of TiO_2. The characteristic peaks for CNTs at $2\theta = 26.0^\circ$ and 43.4° were not observed for 1.25–10 wt% MWCNT-TiO_2, which is different from the previous observation [24]. This phenomenon could be attributed to the good dispersion of MWCNTs in the nanocomposite after surface functionalization in nitrate solution [21]. Average crystal sizes calculated using Scherrer equation [25] from the broadening of the (101) peaks of the anatase are 18.1, 12.8, 12.1, 12.9, 12.6, and 11.8 nm for TiO_2 and 1.25~20 wt% MWCNT-TiO_2, respectively (see Table 1). The small grain of TiO_2 nanoparticles in MWCNT-TiO_2 may be attributed to restricted direct contact of grains due to the presence of MWCNTs.

As can be observed from Figure 2(b), even for MWCNT-TiO_2 calcined at 800°C for 5 h, the XRD pattern shows that all of the crystal phases are still anatase; no peak of rutile appears. Average crystal sizes calculated from the broadening of the (101) peaks of the anatase are 11.6, 12.9, 13.6, 17.8, and 32.9 nm for the 5 wt% MWCNT-TiO_2 as-synthesized and calcined at 400, 500, 600, and 800°C, respectively. These results suggest that MWCNTs in the nanocomposite probably inhibit the phase transformation of TiO_2 from amorphous phase to anatase phase and lead to a higher thermal stability.

To estimate the real content of MWCNTs in composites, 1.25–10 wt% MWCNT-TiO_2 were analyzed by TGA technique. The results shown in Table 1 suggest that the MWCNT/TiO_2 ratios estimated before the synthesis of the MWCNT-TiO_2 were consistent with the results obtained from TGA analysis. Therefore, negligible losses of MWCNTs occurred during the nanocomposite preparation procedure, which is in accordance with the results of Raman analysis on 5 wt% MWCNT-TiO_2 [21]. The BET specific surface areas and pore volumes of the samples are summarized in Table 1. Compared with mesoporous TiO_2 nanoparticles prepared via hydrothermal processes [26], there is a rapid decrease in both BET surface area (from 318 to 111 m^2/g) and total volume (from 0.61 to 0.35 cm^3/g) of TiO_2 nanoparticles after modification with 1.25 wt% MWCNT, which could be due to the close-packed structure between TiO_2 nanoparticles and MWCNTs. With increasing MWCNT content, the BET surface area of MWCNT-TiO_2 decreased firstly and then increased, which can be attributed to the destruction of close-packing due to the self-agglomeration of MWCNTs or TiO_2 nanoparticles at high content.

The UV-vis spectra of MWCNT-TiO_2 display a similar absorption edge to TiO_2 (Figure 3), but an apparent enhancement of absorption throughout the visible-light region can be observed even for the nanocomposite containing 1.25 wt% MWCNTs. A correlation between the MWCNTs amount and absorption changes in the UV-vis spectra obviously features the enhancement of visible-light absorption upon increasing the MWCNT content; that is, the adsorption intensity of the present MWCNT-TiO_2 continuously increased with enhancing MWCNT content owing to its good dispersion.

Control experiments showed no appreciable H_2 evolution in the absence of either photocatalyst or irradiation under visible-light or full spectra irradiation. H_2 generation rates over 5 wt% MWCNT + TiO_2 (a simple mixture of MWCNTs and TiO_2 nanoparticles), 5 wt% MWCNT-TiO_2, TiO_2, and MWCNTs under the visible-light and full spectra irradiation are shown in Figure 4. The pristine TiO_2 and MWCNTs as well as the MWCNT + TiO_2 demonstrate no appreciable H_2 evolution under the visible-light irradiation, whereas

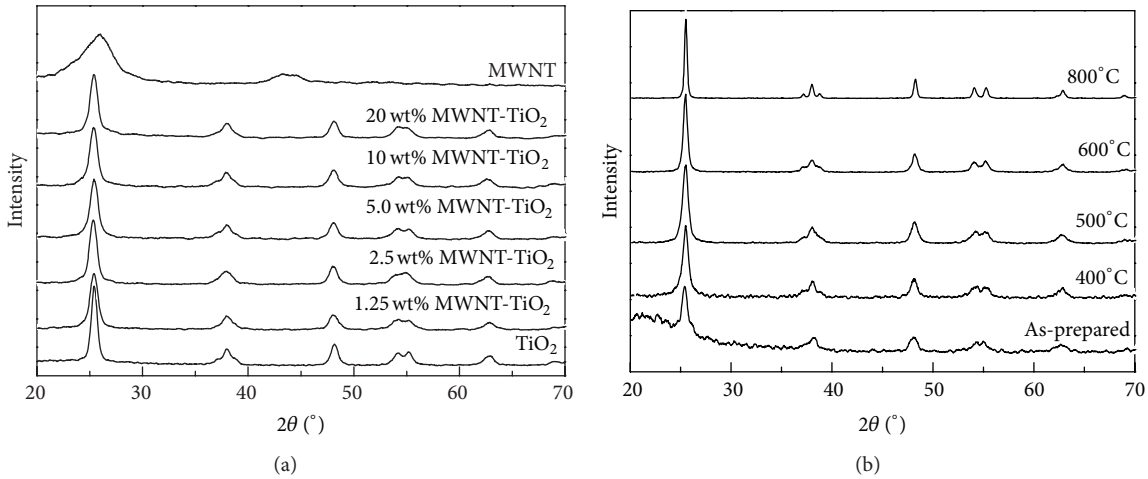

Figure 2: XRD patterns of MWCNT, TiO_2, and MWCNT-TiO_2 with (a) different MWCNT content; (b) 5 wt% MWCNT and calcination at different temperatures.

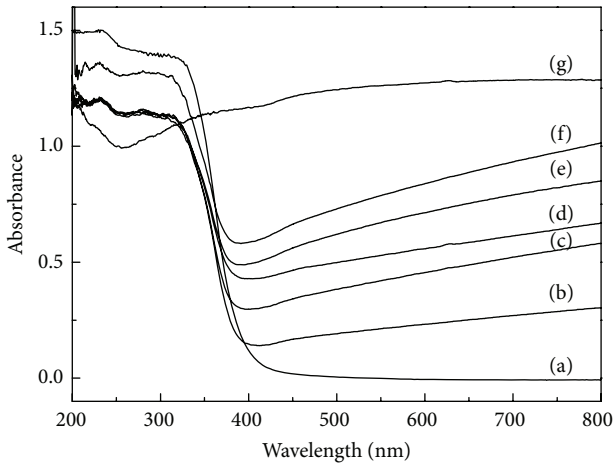

Figure 3: DRS patterns of MWCNT, TiO_2, and MWCNT-TiO_2 with different MWCNT content. (a) TiO_2; (b) 1.25 wt%; (c) 2.5 wt%; (d) 5 wt%; (e) 10 wt%; (f) 20 wt%; (g) MWCNT.

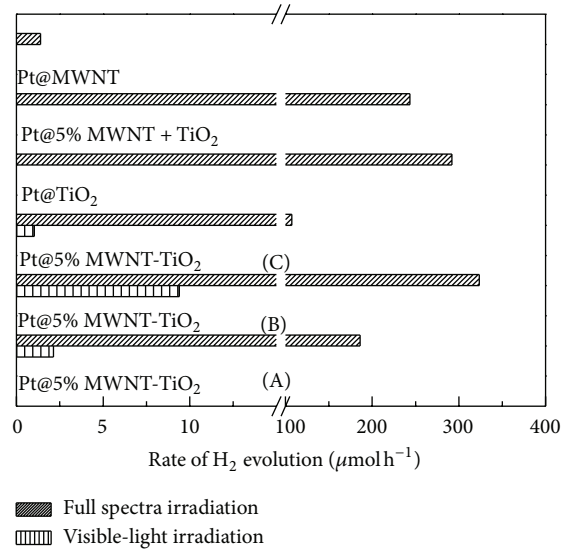

Figure 4: H_2 evolution efficiency over MWCNT, TiO_2, and various photocatalysts containing MWCNT and TiO_2 under visible-light ($\lambda > 420$ nm) and full spectra irradiation. Conditions: 1 wt% Pt-loading; 15 vol % TEOA solution (100 mL); light source, 300 W Xe-lamp. MWCNTs + TiO_2: MWCNTs and TiO_2 nanoparticles were simply mixed together.

MWCNT-TiO_2 (A, B, and C) exhibits various H_2 generation rates, suggesting the importance of chemical linking between MWCNTs and TiO_2 for their visible-light-driven photoactivity [27]. The pretreatment of MWCNTs has a strong effect on the photocatalytic H_2 evolution efficiency over MWCNT-TiO_2. MWCNT-TiO_2 (B) demonstrates the highest H_2 evolution rate under both visible-light and full spectra irradiation.

Different oxidizing reagents possess different degrees of oxidation power, which would purify and decorate MWCNTs with oxygen-containing groups or even destroy their nanotube structure [28]. It is reported that MWCNT bundles appear exfoliated and curled after treatment with strong oxidative environment such as refluxing in nitric acid or stirring in piranha (mixture of sulphuric acid 96 wt% and hydrogen peroxide 30 wt% in ratio 70 : 30) [29]. Comparing the method of refluxing in nitric acid with that of sonicating in a mixture of sulfuric acid and nitric acid, the method of refluxing in nitrate solution provides a moderate oxidation that would generate oxygen-containing groups but would not destroy the MWCNTs structure. Therefore, MWCNT-TiO_2 (B) exhibited the highest photoactivity.

As demonstrated in Figure 5, MWCNT-TiO_2 exhibits no photocatalytic activity until the MWCNT content enhanced to 3.5 wt% under visible-light irradiation. After that, its photocatalytic H_2 evolution efficiency increases firstly

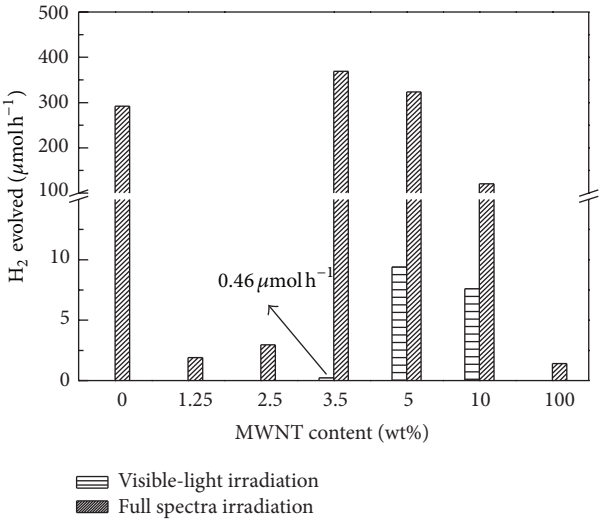

FIGURE 5: The rate of H_2 evolution on MWCNT-TiO_2 nanocomposites with different MWCNT content under visible-light (λ > 420 nm) and full spectra irradiation. Conditions: 1 wt% Pt-loading; 15 vol % TEOA solution (100 mL); light source, 300 W Xe-lamp.

and then decreases slightly with further enhancement of the MWCNT content. The maximum efficiency is achieved at 5 wt% MWCNT-TiO_2 under visible-light irradiation.

It is believed that TiO_2 nanoparticles could directly grow on the surface of the functionalized MWCNTs through the hydrothermal treatment [21]. As shown in Figure 6, no MWCNTs were found in the SEM micrograph of 2.5 wt% MWCNT-TiO_2, which can be attributed to the fact that MWCNTs are embedded inside the nanocomposite by TiO_2 nanoparticles, resulting from the direct growth of TiO_2 on the surface of MWCNTs. For 5 wt% MWCNT-TiO_2, MWCNTs can be observed on the surface of nanocomposite owing to the increase of MWCNT content. These observations can fairly explain the effect of MWCNT content on the visible-light-induced photoactivity. For the MWCNT-TiO_2 with MWCNT content less than 3.5 wt%, MWCNTs embedded inside the nanocomposite cannot be irradiated and excited by visible-light, and thus no visible-light-induced photoactivity was observed [30]. As the visible-light absorbent and sensitizer, higher MWCNT content means more efficient visible-light absorption, and more photogenerated electrons can be transferred to TiO_2; TiO_2 also plays an important role in the separation of photogenerated carriers: the electrons can be transferred from TiO_2 to the loaded Pt. It is reported [31] that the electrical conductivity in the interfacial contact between graphene and photocatalyst components is vital to the overall photocatalytic H_2 production. In addition, unintentional doping of TiO_2 may happen under annealing at 400°C [32, 33], which can increase the visible-light absorbance of TiO_2 and MWCNT-TiO_2. Therefore, there exists an optimal ratio of MWCNT to TiO_2 for achieving excellent electrical conductivity in the nanocomposites and significant photoactivity for H_2 evolution [30].

Under full spectra irradiation, MWCNT-TiO_2 with small MWCNT contents (1.25 wt% and 2.5 wt%) exhibits lower photoactivity than the pure titania, whereas 5 wt% and 3.5 wt% MWCNT-TiO_2 demonstrate the better and the best photoactivity, respectively. Carbon materials such as graphene, C_{60}, and CNT can act as electron traps due to their high electron affinities [31, 34, 35], which would be functionalized as charge separators and enhance the photoactivity [30, 36]. However, as discussed above, for the MWCNT-TiO_2 with MWCNT content less than 3.5 wt%, MWCNTs embedded inside the nanocomposite could act as recombination center of electron and holes, resulting in a reduced photoactivity under full spectra irradiation.

It is well understood that the hydrothermal temperature plays an important role in the morphology, crystallinity, and particle size of TiO_2 [37], which are related to the photoactivity. The effect of hydrothermal temperature on the H_2 generation rate was evaluated under visible-light irradiation. As demonstrated in Figure 7, the H_2 generation rate over 5 wt% MWCNT-TiO_2 increases with the enhanced hydrothermal temperature before 140°C and decreases afterwards under both visible-light and full spectra irradiation. The highest H_2 generation rate of 15.1 μmol·h^{-1} under visible-light irradiation was obtained with 140°C hydrothermal treatment, whereas that of 323.7 μmol·h^{-1} under full spectra irradiation was obtained with 100°C hydrothermal treatment.

The above experimental results could be rationalized by the following discussions. As can be seen from Figure 8, the XRD patterns of 5 wt% MWCNT-TiO_2 derived from different hydrothermal temperatures confirm the fact that the crystallinity of MWCNT-TiO_2 increases with enhancing hydrothermal temperature. It can be calculated using Scherrer equation [25] that average crystal sizes of the anatase are 8.3, 12.9, 15.7, and 26.7 nm for the 5 wt% MWCNT-TiO_2 with hydrothermal temperature of 80, 100, 140, and 180°C, respectively [38]. Under visible-light irradiation, MWCNTs, as a photosensitizer, can absorb visible-light and the photogenerated electrons (e^-) can be excited from the VB to CB of the MWCNT [39]. TiO_2, as the "bridge" between MWCNTs and loaded Pt, would transfer the photogenerated electrons from MWCNT to Pt nanoparticles to generate H_2 from water reduction [40]. As the electron acceptor and transfer station, TiO_2 with high crystallinity and tight combination with MWCNTs could benefit the electron injections and suppress the electron-hole recombination. On the other hand, high crystallinity of TiO_2 would inevitably lead to large crystal size and particle size, which would lead to a high electron-hole recombination rate owing to the long distance for electron transfer. As a result, 5 wt% MWCNT-TiO_2 derived from hydrothermal treatment at 140°C has the highest photoactivity under visible-light irradiation.

Under full spectra irradiation, photocatalytic H_2 generation over TiO_2 irradiated by UV light would make the best part comparing to that over MWCNT-TiO_2 irradiated by visible-light. 5 wt% MWCNT-TiO_2 derived from hydrothermal treatment at 100°C possesses moderate crystal size of anatase, resulting in the highest photoactivity due to the large surface area of MWCNT-TiO_2 and low electron-hole recombination rate.

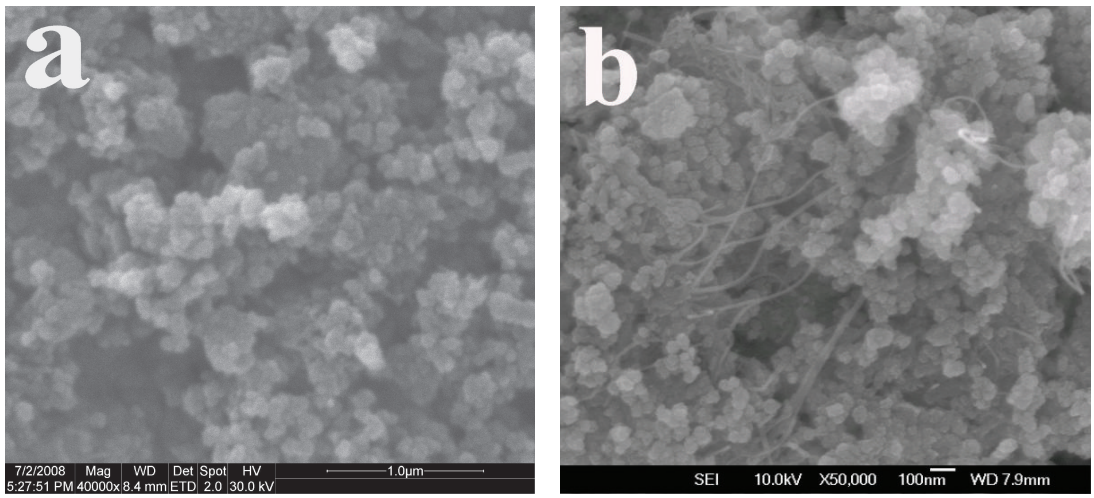

(a) (b)

Figure 6: SEM micrographs of 2.5 wt% (a) and 5 wt% (b) MWCNT-TiO_2 nanocomposite.

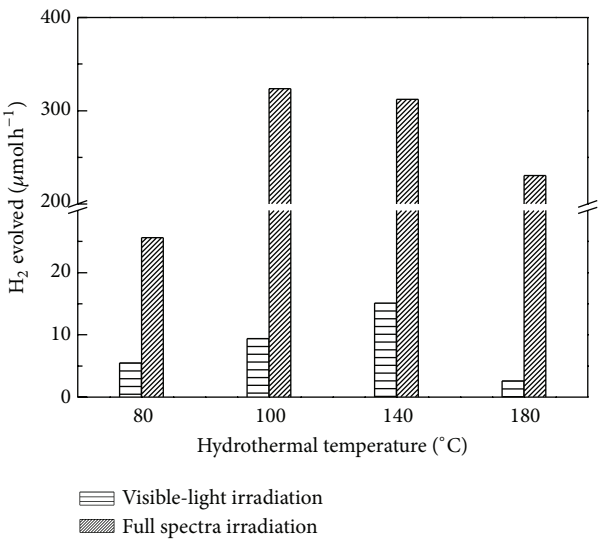

Figure 7: Effect of hydrothermal temperature on photocatalytic H_2 production over 5 wt% MWCNT-TiO_2.

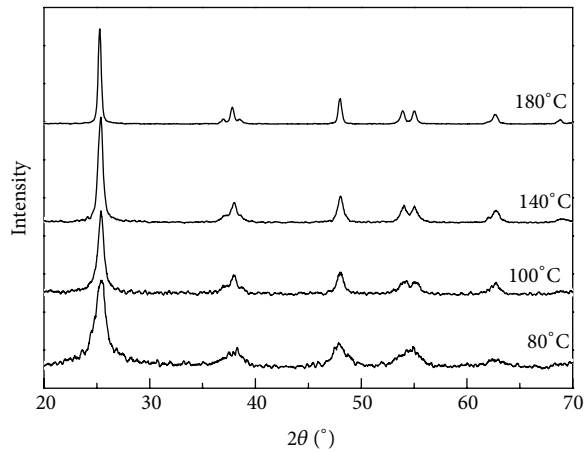

Figure 8: XRD patterns of 5 wt% MWCNT-TiO_2 derived from different hydrothermal temperatures for 72 h.

The photocatalytic activities for H_2 production over 5 wt% MWCNT-TiO_2 upon incident light with different wavelength were investigated. MWCNT-TiO_2 shows a relatively wide photoresponse under monochromatic light of wavelength ranging from 350 to 475 nm (Figure 9), which is consistent with the experimental results obtained with visible-light irradiation (see Figure 4). The apparent quantum efficiency (AQE) of MWCNT-TiO_2 as a function of the wavelength of the incident light was calculated according to the data in Figure 9. MWCNT-TiO_2 demonstrates high quantum efficiency upon irradiation with wavelengths of 420 and 475 nm (4.4% and 3.7%, resp.). With respect to the wide adsorption band in the entire visible-light region (Figure 3), a panchromatic photocatalytic activity could be expected for 5 wt% MWCNT-TiO_2. However, no appreciable H_2 evolution is showed upon irradiation with wavelength longer than 500 nm. As demonstrated in our earlier study, not all MWCNTs in the nanocomposite are bound with TiO_2 nanoparticles, owing to the limited hydroxyl and carboxyl groups generated on the MWCNTs after the functionalization [21]. Therefore, the absorption band between 400 and 800 nm of MWCNT-TiO_2 nanocomposite probably is a combination of the absorption spectrum of both MWCNT-TiO_2 and uncoupled MWCNT, which would absorb light with wavelength longer than 500 nm but cannot be excited to generate electron-hole pairs. On the other hand, the energy of the incident light at longer wavelength dramatically decreased, which would inevitably depress the photoactivity over MWCNT-TiO_2. Furthermore, the photoactivity of TiO_2 under UV light irradiation is enhanced after coupling with MWCNT. The quantum efficiencies for H_2 production over

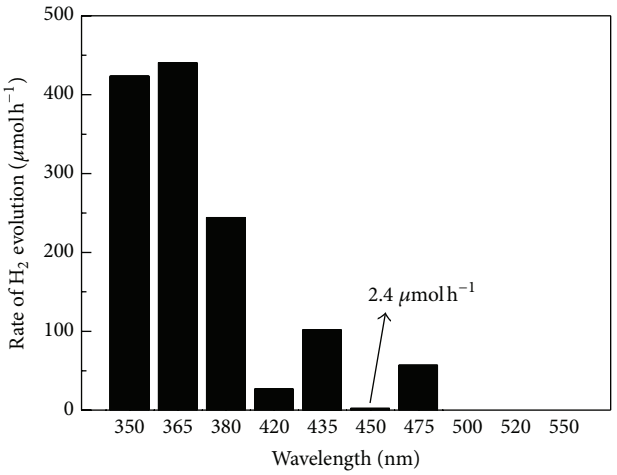

FIGURE 9: The dependence of photocatalytic activities for H_2 production over 5 wt% MWCNT-TiO_2 nanocomposite upon wavelength (controlled via cut-off filters).

P25 TiO_2, mesoporous TiO_2, and MWCNT-TiO_2 at 350 nm were measured to be 1.9, 2.5, and 3.8%, respectively. These phenomena were consistent with the previous discussion that MWCNTs could increase the carrier separation efficiency during photocatalytic process under full spectra irradiation.

4. Conclusions

A series of MWCNT-TiO_2 nanocomposites with different types of functionalized MWCNTs were synthesized through hydrothermal process and characterized by XRD, DRS, SEM, TGA, and BET techniques. The effects of pretreatment methods on MWCNT, MWCNT content, and hydrothermal temperature on the photocatalytic hydrogen evolution efficiency over MWCNT-TiO_2 nanocomposite were investigated. MWCNTs have a good dispersion in the nanocomposite, which inhibit grain growth of TiO_2 and improve its thermal stability. Appropriate pretreatment on MWCNTs could generate oxygen-containing groups, which would become the anchoring sites with TiO_2 nanoparticles in the nanocomposite. However, chemical pretreatment with strong oxidative agents would destroy the intrinsic structure of MWCNTs, which is not beneficial for a high photocatalytic activity. The best photocatalytic activity was observed for the MWCNT-TiO_2 nanocomposite with a 5% weight ratio under visible-light irradiation. The photocatalytic activity of MWCNT-TiO_2 is related to the crystallinity of TiO_2, link type between MWCNT and TiO_2, and MWCNT content. A wide range of photoresponse from 350 to 475 nm is observed with high quantum efficiency. Upon irradiation with wavelengths of 420 and 475 nm, the quantum efficiency is 4.4% and 3.7%, respectively. The above experimental results indicate that the present MWCNT-TiO_2 nanocomposite is a promising photocatalyst with good thermal stability, chemical stability under UV light irradiation, and visible-light-induced photoactivity.

Conflict of Interests

The authors declare that there is no conflict of interests regarding the publication of this paper.

Acknowledgments

The research was financially supported by the Natural Science Foundation of China (20973128, 21271146, and 21307035), Natural Science Foundation of Hubei Province (2011CDB139), and Fundamental Research Funds for Central Universities of China (2013PY112).

References

[1] A. Kudo, "Development of photocatalyst materials for water splitting," *International Journal of Hydrogen Energy*, vol. 31, no. 2, pp. 197–202, 2006.

[2] X. B. Chen, S. H. Shen, L. J. Guo, and S. S. Mao, "Semiconductor-based photocatalytic hydrogen generation," *Chemical Reviews*, vol. 110, no. 11, pp. 6503–6570, 2010.

[3] M. Kitano and M. Hara, "Heterogeneous photocatalytic cleavage of water," *Journal of Materials Chemistry*, vol. 20, no. 4, pp. 627–641, 2010.

[4] X. Liu, Z. Q. Liu, J. Zheng et al., "Characteristics of N-doped TiO_2 nanotube arrays by N_2-plasma for visible light-driven photocatalysis," *Journal of Alloys and Compounds*, vol. 509, no. 41, pp. 9970–9976, 2011.

[5] D. Jiang, Y. Xu, B. Hou, D. Wu, and Y. Sun, "Synthesis of visible light-activated TiO_2 photocatalyst via surface organic modification," *Journal of Solid State Chemistry*, vol. 180, no. 5, pp. 1787–1791, 2007.

[6] H. Park, Y. K. Kirn, and W. Choi, "Reversing CdS preparation order and its effects on photocatalytic hydrogen production of CdS/Pt-TiO_2 hybrids under visible light," *The Journal of Physical Chemistry C*, vol. 115, pp. 6141–6148, 2011.

[7] S. In, A. Orlov, R. Berg et al., "Effective visible light-activated B-doped and B,N-codoped TiO_2 photocatalysts," *Journal of the American Chemical Society*, vol. 129, no. 45, pp. 13790–13791, 2007.

[8] S. Bingham and W. A. Daoud, "Recent advances in making nano-sized TiO_2 visible-light active through rare-earth metal doping," *Journal of Materials Chemistry*, vol. 21, no. 7, pp. 2041–2050, 2011.

[9] H. Gao, C. Liu, H. E. Jeong, and P. Yang, "Plasmon-enhanced photocatalytic activity of iron oxide on gold nanopillars," *ACS Nano*, vol. 6, no. 1, pp. 234–240, 2012.

[10] Z. Liu, W. Hou, P. Pavaskar, M. Aykol, and S. B. Cronin, "Plasmon resonant enhancement of photocatalytic water splitting under visible illumination," *Nano Letters*, vol. 11, no. 3, pp. 1111–1116, 2011.

[11] Z. Zhan, J. An, H. Zhang, R. V. Hansen, and L. Zheng, "Three-dimensional plasmonic photoanodes based on Au-embedded TiO_2 structures for enhanced visible-light water splitting," *ACS Applied Materials & Interfaces*, vol. 6, no. 2, pp. 1139–1144, 2014.

[12] A. Primo, A. Corma, and H. Garcia, "Titania supported gold nanoparticles as photocatalyst," *Physical Chemistry Chemical Physics*, vol. 13, pp. 886–910, 2011.

[13] K. Awazu, M. Fujimaki, C. Rockstuhl et al., "A plasmonic photocatalyst consisting of silver nanoparticles embedded in

titanium dioxide," *Journal of the American Chemical Society*, vol. 130, no. 5, pp. 1676–1680, 2008.

[14] D. B. Ingram and S. Linic, "Water splitting on composite plasmonic-metal/semiconductor photoelectrodes: evidence for selective plasmon-induced formation of charge carriers near the semiconductor surface," *Journal of the American Chemical Society*, vol. 133, no. 14, pp. 5202–5205, 2011.

[15] T. Ihara, M. Miyoshi, Y. Iriyama, O. Matsumoto, and S. Sugihara, "Visible-light-active titanium oxide photocatalyst realized by an oxygen-deficient structure and by nitrogen doping," *Applied Catalysis B: Environmental*, vol. 42, no. 4, pp. 403–409, 2003.

[16] X. B. Chen, L. Liu, P. Y. Yu, and S. S. Mao, "Increasing solar absorption for photocatalysis with black hydrogenated titanium dioxide nanocrystals," *Science*, vol. 331, no. 6018, pp. 746–750, 2011.

[17] H. Y. Chang, W. J. Tzeng, C. H. Lin, and S. Y. Cheng, "Ionic compounds lamination reaction and characteristics of photosensitive copper indium sulfide on titania nanotube arrays," *Journal of Alloys and Compounds*, vol. 509, no. 35, pp. 8700–8706, 2011.

[18] R. Leary and A. Westwood, "Carbonaceous nanomaterials for the enhancement of TiO_2 photocatalysis," *Carbon*, vol. 49, no. 3, pp. 741–772, 2011.

[19] B. Ahmmad, Y. Kusumoto, S. Somekawa, and M. Ikeda, "Carbon nanotubes synergistically enhance photocatalytic activity of TiO_2," *Catalysis Communications*, vol. 9, no. 6, pp. 1410–1413, 2008.

[20] Y. Ou, J. D. Lin, S. M. Fang, and D. W. Liao, "MWNT–TiO_2:Ni composite catalyst: a new class of catalyst for photocatalytic H_2 evolution from water under visible light illumination," *Chemical Physics Letters*, vol. 429, pp. 199–203, 2006.

[21] K. Dai, T. Y. Peng, D. N. Ke, and B. Q. Wei, "Photocatalytic hydrogen generation using a nanocomposite of multi-walled carbon nanotubes and TiO_2 nanoparticles under visible light irradiation," *Nanotechnology*, vol. 20, no. 12, Article ID 125603, 2009.

[22] B. Kim and W. M. Sigmund, "Functionalized multiwall carbon nanotube/gold nanoparticle composites," *Langmuir*, vol. 20, no. 19, pp. 8239–8242, 2004.

[23] P. Zeng, Q. G. Zhang, X. Zhang, and T. Y. Peng, "Graphite oxide-TiO_2 nanocomposite and its efficient visible-light-driven photocatalytic hydrogen production," *Journal of Alloys and Compounds*, vol. 516, pp. 85–90, 2012.

[24] W. D. Wang, P. Serp, P. Kalck, and J. L. Faria, "Visible light photodegradation of phenol on MWNT-TiO_2 composite catalysts prepared by a modified sol-gel method," *Journal of Molecular Catalysis A: Chemical*, vol. 235, no. 1-2, pp. 194–199, 2005.

[25] X. H. Huang, Z. Y. Zhan, X. Wang et al., "Rayleigh-instability-driven simultaneous morphological and compositional transformation from Co nanowires to CoO octahedra," *Applied Physics Letters*, vol. 97, Article ID 203112, 2010.

[26] T. Peng, D. Zhao, K. Dai, W. Shi, and K. Hirao, "Synthesis of titanium dioxide nanoparticles with mesoporous anatase wall and high photocatalytic activity," *The Journal of Physical Chemistry B*, vol. 109, no. 11, pp. 4947–4952, 2005.

[27] G. M. An, W. H. Ma, Z. M. Sun et al., "Preparation of titania/carbon nanotube composites using supercritical ethanol and their photocatalytic activity for phenol degradation under visible light irradiation," *Carbon*, vol. 45, no. 9, pp. 1795–1801, 2007.

[28] W. H. Lee, S. J. Kim, W. J. Lee, J. G. Lee, R. C. Haddon, and P. J. Reucroft, "X-ray photoelectron spectroscopic studies of surface modified single-walled carbon nanotube material," *Applied Surface Science*, vol. 181, no. 1-2, pp. 121–127, 2001.

[29] V. Datsyuk, M. Kalyva, K. Papagelis et al., "Chemical oxidation of multiwalled carbon nanotubes," *Carbon*, vol. 46, no. 6, pp. 833–840, 2008.

[30] J. G. Yu, T. T. Ma, and S. W. Liu, "Enhanced photocatalytic activity of mesoporous TiO_2 aggregates by embedding carbon nanotubes as electron-transfer channel," *Physical Chemistry Chemical Physics*, vol. 13, pp. 3491–3501, 2011.

[31] Q. J. Xiang and J. G. Yu, "Graphene-based photocatalysts for hydrogen generation," *The Journal of Physical Chemistry Letters*, vol. 4, pp. 753–759, 2013.

[32] X. H. Huang, C. B. Tay, Z. Y. Zhan et al., "Universal photoluminescence evolution of solution-grown ZnO nanorods with annealing: important role of hydrogen donor," *CrystEngComm*, vol. 13, no. 23, pp. 7032–7036, 2011.

[33] X. H. Huang, Z. Y. Zhan, K. P. Pramoda, C. Zhang, L. X. Zheng, and S. J. Chua, "Correlating the enhancement of UV luminescence from solution-grown ZnO nanorods with hydrogen doping," *CrystEngComm*, vol. 14, no. 16, pp. 5163–5165, 2012.

[34] K. Dai, Y. Yao, H. Liu, I. Mohamed, H. Chen, and Q. Y. Huang, "Enhancing the photocatalytic activity of lead molybdate by modifying with fullerene," *Journal of Molecular Catalysis A: Chemical*, vol. 374, pp. 111–117, 2013.

[35] C. Liu, H. Chen, K. Dai, A. Xue, and Q. Huang, "Synthesis, characterization, and its photocatalytic activity of double-walled carbon nanotubes-TiO_2 hybrid," *Materials Research Bulletin*, vol. 48, no. 4, pp. 1499–1505, 2013.

[36] K. Dai, X. H. Zhang, K. Fan, T. Y. Peng, and B. Q. Wei, "Hydrothermal synthesis of single-walled carbon nanotube—TiO_2 hybrid and its photocatalytic activity," *Applied Surface Science*, vol. 270, pp. 238–244, 2013.

[37] D. S. Kim and S. Y. Kwak, "The hydrothermal synthesis of mesoporous TiO_2 with high crystallinity, thermal stability, large surface area, and enhanced photocatalytic activity," *Applied Catalysis A: General*, vol. 323, pp. 110–118, 2007.

[38] S. Bangkedphol, H. E. Keenan, C. M. Davidson, A. Sakultantimetha, W. Sirisaksoontorn, and A. Songsasen, "Enhancement of tributyltin degradation under natural light by N-doped TiO_2 photocatalyst," *Journal of Hazardous Materials*, vol. 184, no. 1–3, pp. 533–537, 2010.

[39] O. Akhavan, M. Abdolahad, Y. Abdi, and S. Mohajerzadeh, "Synthesis of titania/carbon nanotube heterojunction arrays for photoinactivation of *E. coli* in visible light irradiation," *Carbon*, vol. 47, no. 14, pp. 3280–3287, 2009.

[40] T. Puangpetch, T. Sreethawong, and S. Chavadej, "Hydrogen production over metal-loaded mesoporous-assembled $SrTiO_3$ nanocrystal photocatalysts: effects of metal type and loading," *International Journal of Hydrogen Energy*, vol. 35, no. 13, pp. 6531–6540, 2010.